Journal of Sound and Vibration (1998) **216**(4), 553–570
Article No. sv951713

VIBRO–ACOUSTIC ANALYSIS AND IDENTIFICATION OF DEFECTS IN ROTATING MACHINERY, PART I: THEORETICAL MODEL

N. Hamzaoui, C. Boisson and C. Lesueur

Laboratoire Vibrations Acoustique Bt 303 *INSA*, 20 *Avenue Albert Einstein*, 69621 *Villeurbanne Cedex*, *France*

(*Received* 26 *July* 1995)

The objective of our work is the association of vibratory diagnosis knowledge with an acoustic part including frequential and spatial criteria for the identification of noise sources in rotating machinery. To control parameters for this difficult problem, one proceeds by stages and with confrontation of theoretical and experimental methods. This paper presents the theoretical modelling of a rotor on bearings system, with a simulation of several defects such as misalignment, imbalance and defective bearings. Pressure field calculations are performed with the help of an effective method based on modelling a structure by a set of point sources placed on the radiating surface.

1. INTRODUCTION

Two kinds of excitations can produce noise in rotating machinery; excitations due to primary sources, and excitations due to manufacturing defects. It is difficult to act on the primary sources or functional loads as they are specific to a machine; in this paper, the effects of classical manufacturing defects are discussed. These defects are inherent in both the manufacturing quality and the configuration of the machine. They are caused by the machine's rotating parts (rotors, disks, bearings, gears . . .) and create concentrated or distributed loads that produce vibrations and noise. These vibrations depend on the machine itself through the transfer function while the noise is a function of the machine environment.

This noise can come from (1) vibrating surface radiation, and (2) the aeroacoustic response of the system to turbulent fluid motion. One's goal is to predict the noise generated by this type of excitation in the following areas: the defect identification through acoustic analysis (this could further lead to machine acoustic supervision); noise reduction by means of local actions; development of a procedure for conceiving quieter machines.

Many problems appear in this kind of study. Among these two are predominant; first, the geometrical complexity of the machine and secondly, on the experimental level the difficulty in isolating a particular defect whose vibrating characteristics are time dependant because of wear.

0022–460X/98/390553 + 18 $30.00/0

In this paper, the basic foundations that yield the formulation of the model is presented, along with the general hypotheses made; two classical defects, imbalance and shaft misalignment are then examined.

Imbalance is a condition in which the center of mass or a rotating assembly, such as the shaft and its fixed components (disk, blades . . .) is not coincident with the center of rotation. This phenomenon has been thoroughly studied [1–6]. As a result of imbalance, vibrations are generated. They can be analyzed through spectral analysis and some solutions involving the balancing of the rotating elements exist.

Shaft misalignment, which can determine a machine's reliability, is a condition in which the shaft of the driving machine and the shaft of the driven machine are not on the same centerline. It is in general a combination of both parallel and angular misalignments in the vertical and horizontal directions. Flexible couplings are commonly used to accommodate this fault that can severely damage bearings and gears.

Xu and Marangoni [4, 5], recently pursued a vibration analysis based on a theoretical model and its validation. They showed the adequacy of knowing both the system natural frequencies and the rotor running speed, so that shaft misalignment tends to show up in the frequency domain as a series of harmonics of the shaft running speed, the ($2 \times$ r.p.m.) harmonic being predominant.

The closer these harmonics are to the systems' natural frequencies, the higher is the magnitude of these harmonics. Xu and Marangoni also studied the response to an imbalance–misalignment coupling, more weight being given to the misalignment fault. As a result, they noticed that the response in the frequency domain decreases as imbalance increases.

Dewell and Mitchell [7] analyzed the vibration frequencies for a misaligned metallic disk flexible coupling. Their experimental results obtained by the means of spectral analysis show that all the theoretically predicted vibration frequencies actually appear with the $2\times$ and $4\times$ running speed components showing the largest changes as misalignment increases. Gibbons (quoted in reference [10]) described the reaction forces generated by shaft misalignment for non-lubricated couplings, which are seeing increased usage in industry.

Krodkiewski and Ding [8, 9] developed a general approach for on-site identification of the misalignment of a multi-bearing–rotor system (e.g., a turbo generator unit). This identification, which enables the calculation to be made of the dynamic forces acting on the journal bearings for each instant of time t, is based on a non-linear mathematical model of the system and the knowledge of the relative transverse positions of the bearings with respect to the shaft. The mathematical model includes the dynamic properties of rotors their foundations and supporting structures as well as the non-linear properties of the oil bearings. The latter are modelled on the basis of Reynolds' equation that yields the expression for pressure distribution which is used as a non-linear excitation in the vibration equation system. The other excitations consist of the static load and external forces. Shaft misalignment is introduced as a constant vector representing the bearing transverse positions with respect to the inertial co-ordinate system which is added to the rotor absolute co-ordinates; it is therefore equivalent to an

additional force in the system of equations. The specification of the misalignment configuration parameters experimentally applied to a four-bearing rotor installation is developed in the mathematical model. In order to perform numerical calculations the identification of the rotor orbits is also necessary. For this type of journal bearing, the characterization of misalignment in the frequency domain is revealed by the increase of the vibration response for the 1/2 running speed and the appearance of instability signs. Morel [2] treated these phenomena by realizing measurements on industrial structures enabling him to make diagnoses.

These mechanical faults are thus modelled by excitation forces which are applied to a system whose vibration transfer functions depends on the running speed and time (non-linear bearings stiffness).

Such methods as Runge–Kutta for non-linear systems [8], finite elements method [1], modal decomposition, Rayleigh–Ritz [1, 4] have been used to obtain numerically this transfer function. As far as acoustic effects are concerned, their studies are still inadequate and very few analyses have been carried out up to now.

There seems to be a physical relationship between the mechanical faults and the noise produced by a machine. One would therefore tend to associate vibration analyses results, that detect the main vibration causes due to internal defects, with an acoustic study whose goal is to characterize these defects in space and in time.

As these machines are complex, the present procedure is based on a simplification of the model of the phenomena that involve vibration response measurements in order to predict the acoustic radiated pressure or power.

Perreira and Dubowski [10] developed techniques for the prediction of noise levels of linked mechanical systems with elastic elements and connection clearances. In particular, they examined the case of a beam on two journal bearings modeled by springs in tension/compression and viscous damping. The prediction made is based on a simplified expression of the Helmholtz integral equation and leads to the formulation of far field radiation. This simplification, which is valid only in some cases, neglects the surface pressure contribution (dipolar effect) with respect to vibration speeds (monopolar effect). The authors conclude that the noise generation process is strongly related to connection clearances, link elasticity and bearing forces. Noise levels increase with the clearances in the model due to impacts on the bearings.

Finally the identification of radiated noise in rotating machinery seems to be very important to predict the machine's quality and reliability in order to assess noise control. Noise prediction along with vibration characterization will lead to a thorough determination of the main vibration sources due to internal defects both in space and in time.

By using conclusions made from former studies, the authors undertake in this paper a vibro–acoustical analysis based on a procedure that enables one to consider correctly the problems encountered: a linear model of a motor–journal bearings–rotor system capable of computing mechanical vibrations and noise radiations resulting from imbalance and misalignment is first developed; as a second step, an experimental installation (see Part II) capable of simulating and monitoring mechanical defects from rotating machinery is described.

In this first part, the basic model for the vibro-acoustical analysis is presented, the hypotheses and simulation approaches made, and the results given by the model and the conclusions that can be drawn.

2. MODELLING OF ROTOR DEFECTS

The system consists of a rotor and journal bearings [11]. The journal bearings are modelled by springs which are of two types: springs in translatory motion; springs in rotating motion. The rotor is made of rigid disks and the shaft is modelled by a beam in bending (Figure 1).

2.1. VIBRATING MODEL

Journal bearings stiffnesses are known in both directions X and Z. Ω denotes the rotor angular velocity and θ and Ψ are the angles of the shaft around X and Z due to the beam bending deflection.

Displacements and rotations are given by the following expressions:

$$X(y,t) = \sum_{i=1}^{N} q_i(t) f_i(y) + \sum_{i=0}^{N} p_i(t) g_i(y), \qquad Z(y,t) = \sum_{i=1}^{N} h_i(t) f_i(y) + \sum_{i=0}^{N} t_i(t) g_i(y), \tag{1, 2}$$

$$\theta(y,t) = \partial Z/\partial y, \qquad \psi(y,t) = -\partial X/\partial y,$$

$$f_i(y) = \sin(i\pi y/L), \qquad g_i(y) = \cos(i\pi y/L). \tag{3–6}$$

Lagrange's equations associated with the Rayleigh–Ritz method yield a system of differential equations that describes free motion and whose degree of freedom N is limited:

$$\begin{bmatrix} [M] & 0 \\ 0 & [M] \end{bmatrix} \{\ddot{\delta}\} + \begin{bmatrix} 0 & [-C(\Omega)] \\ [C(\Omega)] & 0 \end{bmatrix} \{\dot{\delta}\} + \begin{bmatrix} [K_x] & 0 \\ 0 & [K_z] \end{bmatrix} \{\delta\} = 0. \tag{7}$$

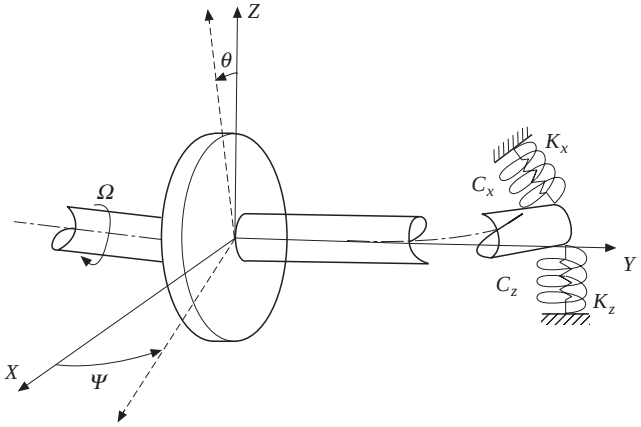

Figure 1. Rotor model. Ω, θ and ψ denote respectively the rotor rotating speed and the rotations from the shaft deflections due to bending around axes X and Z.

Expression (7) can be written as

$$M_A\ddot{\delta} + C_A\dot{\delta} + K_A\delta = 0. \tag{8}$$

The components of matrices $[M]$, $[K_x]$, $[K_y]$ and $[C]$ are of dimension $(2N + 1)$, and

$$\delta = \begin{Bmatrix} q_i \\ p_j \\ h_i \\ t_j \end{Bmatrix}, \qquad i = 1, N, \quad j = 1, N.$$

Solving the homogeneous differential equation system (8) leads to the natural frequencies and modes of the system motion along X and Z when the rotor is either at rest or running. One can then draw Campbell's diagram giving the variation of natural frequencies with the rotor angular velocity and critical speeds of the system.

By using the Q.R. method, one finally obtains the following system:

$$\begin{bmatrix} 0 & -I \\ K_A^{-1}M_A & K_A^{-1}C_A \end{bmatrix} \begin{Bmatrix} \dot{\delta} \\ \delta \end{Bmatrix} = \frac{-1}{r} \begin{Bmatrix} \dot{\delta} \\ \delta \end{Bmatrix}, \quad \text{with} \quad \begin{Bmatrix} \dot{\delta} \\ \delta \end{Bmatrix} = \{x_0\}\, \mathrm{e}^{rt} \tag{9}$$

2.2. VIBRATION RESPONSE TO DEFECTS

The response to excitation forces that characterize defects such as misalignment or imbalance is obtained by developing direct methods (harmonic decomposition). One needs to solve

$$\begin{bmatrix} [M] & 0 \\ 0 & [M] \end{bmatrix} \{\ddot{\delta}\} + \begin{bmatrix} 0 & [-C(\Omega)] \\ [C(\Omega)] & 0 \end{bmatrix} \{\dot{\delta}\} + \begin{bmatrix} [K_x] & 0 \\ 0 & [K_z] \end{bmatrix} \{\delta\} = \{F\}, \tag{10}$$

where $\{F\}$ represents the excitation forces used to model the defects.

Depending on the type of defects, the expression for $\{F\}$ changes.

For imbalance, a mass m_b, a distance d from the axis of a cross-section (of the shaft), induces the imbalance force

$$F_b(\Omega) = \begin{Bmatrix} F_{qi} \\ F_{pi} \\ F_{hi} \\ F_{ti} \end{Bmatrix} = \begin{Bmatrix} m_b d\Omega^2 f_i(lb) \sin(\Omega t) \\ m_b d\Omega^2 g_i(lb) \sin(\Omega t) \\ m_b d\Omega^2 f_i(lb) \cos(\Omega t) \\ m_b d\Omega^2 g_i(lb) \cos(\Omega t) \end{Bmatrix}. \tag{11}$$

Here lb is the Y-coordinate of mb.

For shaft misalignment the defect is complex. It is modelled by superposing harmonic excitations such that the frequencies are proportional to the system angular velocity. This defect also modifies the journal bearings stiffnesses and the rotor dynamic responses at the same time.

Figure 2. Shafts misalignment: (a) parallel; (b) angular.

There are two kinds of misalignment (parallel and angular) located at the coupling between two shafts (see Figure 2) or at the journal bearings (see Figure 3). Misalignment between journals is complex, indeed it depends on the rigidity of the different elements in contact (journals, bearings, rotor) and therefore affects the vibration transfer function of the system.

By taking into consideration observations made from former analyses and from experiments on misalignment, a simplified theoretical model for a misaligned system [12] was studied, whose development is detailed in the Appendix. This analysis is made in order to determine the shape of the force caused by misalignment.

In order to include the rotor vibration behavior with this type of excitation, the general case of an asynchronous excitation was examined where $s\Omega$ denotes the angular velocity located at $Y = l_s$.

By means of a Fourier series decomposition, one obtains $\{F\}$ modelling the misalignment:

$$\{F_D(s\Omega)\} = \begin{Bmatrix} \sum_{n=1}^{\infty} F_n^x f_i(l_s) \sin(ns\Omega t) \\ \sum_{n=1}^{\infty} F_n^x g_i(l_s) \sin(ns\Omega t) \\ \sum_{n=1}^{\infty} F_n^z f_i(l_s) \cos(ns\Omega t) \\ \sum_{n=1}^{\infty} F_n^z g_i(l_s) \cos(ns\Omega t) \end{Bmatrix}. \tag{12}$$

Here F_n^x and F_n^z are the magnitudes of the force F for each frequency $(n \times s\Omega)$ along axes X and Z.

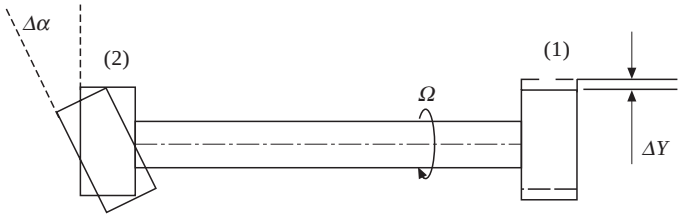

Figure 3. Journals misalignment: (1) parallel; (2) angular.

One observes misalignment where n usually remains less than 6 and s is close to 1 for small values of the angle of misalignment.

For defects in the bearings it is possible to assess values of frequencies where this type of defect appears with a theoretical calculation involving the bearings' characteristics and the rotor running speed. The vibration response to this type of excitation is easily observed by spectrum analyses. It produces a spectrum whose shape is identical to the one describing the system transfer function at the same frequency. In order to simulate this type of defect, one can analyse the response to a mechanical harmonic excitation located at the bearings by monitoring the angular velocity, choosing values proportional to the characterized defect angular velocity, with a prescribed value for Ω.

The corresponding vector $\{F\}$ has the following expression:

$$\{F_R(\omega)\} = \begin{Bmatrix} F_{RX} f_i(l_r) \sin(\omega t) \\ F_{RX} g_i(l_r) \sin(\omega t) \\ F_{RZ} f_i(l_r) \cos(\omega t) \\ F_{RZ} g_i(l_r) \cos(\omega t) \end{Bmatrix}. \tag{13}$$

One can use any of the expressions for $\{F\}$ above or a combination of them (coupling of excitations) in the second member of equation (10). The vibration response is a spectrum with the same shape as the spectrum characterizing the discrete system transfer function. One can therefore analyze the rotor vibrations along axes X and Z as functions of the shaft running speed, the magnitudes and positions in space of the different excitations whether they are coupled or not.

3. NOISE PREDICTION

In the industrial world noise measurements are affected by the machine environment and other noise sources; it is therefore relevant to carry out vibration measurements to assess noise levels.

The procedure consists of a calculation of the acoustic pressure in the outer field based on the knowledge of the structure as a vibrating surface placed above a rigid ground. The fluid medium is air; one can neglect its effects on the structures' behavior.

3.1. GENERAL DESCRIPTION

An envelop S represents the exterior vibrating surface of the machine. S is coupled to an external volume V_e of fluid. This volume V_e is semi-infinite, such that Sommerfeld conditions are respected.

The envelop S is placed above a rigid infinite ground Σ_0 (see Figure 4); the acoustics is then expressed by the following linear equations:

$$\Delta P(M) + k^2 P(M) = 0, \quad M \in V_e;$$

$$(\partial P/\partial n_{M_0})(M_0) = -\mathrm{j}\rho_0 V_n(M_0), \quad M_0 \in S; \qquad (\partial P/\partial n_{M_0})(M_0) = 0, \quad M_0 \in \Sigma_0;$$

$$\text{Sommerfeld conditions.} \tag{14}$$

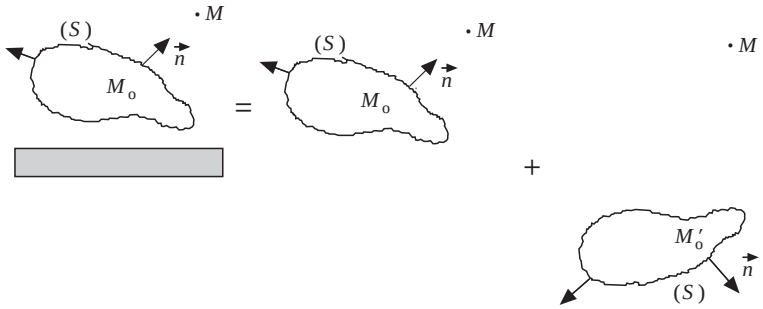

Figure 4. Image source principle applied to acoustic vibrations of structures.

Here $P(M_0)$ is the acoustic pressure at point M_0, $V_n(M_0)$ is the vibration speed at point M_0, ρ_0 is the fluid density, and $\overrightarrow{n_{M_0}}$ is the outward surface normal at point M_0.

To solve this problem, one uses the integral formulation for the acoustic pressure:

$$P(M) = \int\int_s \left(P(M_0) \frac{\partial G(M, M_0)}{\partial n_{M_0}} - \frac{\partial P}{\partial n_{M_0}} (M_0) G(M, M_0) \right) \mathrm{d}S_{M_0}. \tag{15}$$

The Green function $G(M, M_0)$ is a solution of the Helmholtz equation. Its determination is based on the "image source" technique (see Figure 4):

$$G(M, M_0) = G_1(M, M_0) + G_2(M, M_0') = \frac{\mathrm{e}^{-\mathrm{j}kr_1}}{4\pi r_1} + \frac{\mathrm{e}^{-\mathrm{j}kr_2}}{4\pi r_2}. \tag{16}$$

Here

$$r_1 = [(x_M - x_{M_0})^2 + (y_M - y_{M_0})^2 + (z_M - z_{M_0})^2]^{1/2}, \tag{17}$$

$$r_2 = [(x_M - x_{M_0})^2 + (y_M - y_{M_0})^2 + (z_M + z_{M_0})^2]^{1/2}. \tag{18}$$

Numerical methods such as finite elements or boundary elements are necessary to solve this type of problem. A program enabling acoustic calculations to be made from results given by a vibration analysis was developed. This program follows the collocation method using one-node triangular and two-node beam elements. It is well adapted for structures presenting plane geometry such as plates, sets of plates or parallelepipedic boxes.

For an industrial structure having a more complex geometry it is necessary to develop a complex experimental process, generating many sources of errors (types of elements, mesh definition, determination of normal vectors at nodes, interpolation . . .). As a consequence, simplifying assumptions were made that allows one not to affect noise prediction from the qualitative point of view and with a satisfying accuracy in the quantitative predictions.

3.2. SIMPLIFYING ASSUMPTIONS

Equation (15) can be re-expressed as

$$P(M) = \int\int_s \left(P(M_0)\left(\frac{1}{r_1} + \mathrm{j}k\right)\cos\vartheta_1 + \mathrm{j}\rho_0\omega V_n(M_0)\right)\frac{\mathrm{e}^{-\mathrm{j}kr_1}}{4\pi r_1}\,\mathrm{d}S_{M_0}$$

$$+ \int\int_s \left(P(M_0')\left(\frac{1}{r_2} + \mathrm{j}k\right)\cos\vartheta_2 + \mathrm{j}\rho_0\omega V_n(M_0')\right)\frac{\mathrm{e}^{-\mathrm{j}kr_2}}{4\pi r_2}\,\mathrm{d}S_{M_0'}, \quad (19)$$

where

$$\cos\vartheta_1 = (\overrightarrow{M_0M}/r_1)\cdot\vec{n}_{M_0} \quad \text{and} \quad \cos\vartheta_2 = (\overrightarrow{M_0'M}/r_2)\cdot\vec{n}_{M_0'}.$$

For low frequencies, surface pressure can be determined by introducing an hypothesis concerning the dynamics of incompressible fluids. This hypothesis is valid when the acoustic wave length ($\lambda = 2\pi/k$) is much greater than the largest dimension L of the envelop S. It is given by the expression

$$P(M_0) \approx \rho_0 L\,\partial V_n(M_0)/\partial t \approx \mathrm{j}\rho_0\omega L V_n(M_0). \quad (20)$$

Expression (19) then becomes

$$P(M) = \int\int_s \left(\left(\frac{L}{r_1} + \mathrm{j}kL\right)\cos\vartheta_1 + 1\right)\mathrm{j}\rho_0\omega V_n(M_0)\,\frac{\mathrm{e}^{-\mathrm{j}kr_1}}{4\pi r_1}\,\mathrm{d}S_{M_0}$$

$$+ \int\int_s \left(\left(\frac{L}{r_2} + \mathrm{j}kL\right)\cos\vartheta_2 + 1\right)\mathrm{j}\rho_0\omega V_n(M_0')\,\frac{\mathrm{e}^{-\mathrm{j}kr_2}}{4\pi r_2}\,\mathrm{d}S_{M_0'}. \quad (21)$$

Finally at low frequencies ($kL \ll 1$) and under the far field condition ($L/r \ll 1$) the acoustic pressure can be expressed as

$$P(M) = \mathrm{j}\rho_0\omega \int\int_s V_n(M_0)\left(\frac{\mathrm{e}^{-\mathrm{j}kr_1}}{4\pi r_1} + \frac{\mathrm{e}^{-\mathrm{j}kr_2}}{4\pi r_2}\right)\mathrm{d}S_{M_0}. \quad (22)$$

Ones approach is thus based on a monopolar distribution, characterized by vibration speeds (magnitudes and phase shifts) and the radiating surfaces that are produced when the system is discretized. Then

$$\tilde{P}(M) = \mathrm{j}\rho_0\omega \sum_{i=1}^{N_e} |V_i|\,\mathrm{e}^{\mathrm{j}(\varphi_{ref} - \varphi_i)} \int\int_{\Delta S_i} G(M, M_i)\,\mathrm{d}\Delta S_{(M_i)}. \quad (23)$$

φ_{ref} and φ_i denote the reference phase and the phase at point i, respectively.

The advantage of using such an approach is due to the fact that it is easy to set up experimentally and numerical calculations are also simple.

From an exact formulation of the active acoustic intensity, the acoustic power can be expressed as

$$W \approx \sum_{i=1}^{N} \vec{I}_i \vec{n}_i \, \Delta\Gamma_i, \quad \text{where} \quad \vec{I}_i = \tfrac{1}{2} \operatorname{Re}\left(P_i \cdot \frac{1}{\mathrm{j}\rho_0 \omega} \begin{Bmatrix} \partial P_i/\partial x^* \\ \partial P_i/\partial y^* \\ \partial P_i/\partial z^* \end{Bmatrix} \right), \tag{24}$$

and $\vec{I}_i$ is the active acoustic intensity vector. * denotes the complex conjugate and

$$\Gamma \approx \sum_{i=1}^{N} \Delta\Gamma_i$$

is the control surface.

4. VIBRATION CALCULATIONS

When the running speed $\Omega = 0$, the calculation of natural frequencies is equivalent to a beam problem with particular boundary conditions. The comparison between the calculated natural frequencies and the ones given is satisfactory [11].

When $\Omega \neq 0$, the comparison uses examples treated with the finite elements method [1]. Campbell diagrams, giving the variation of natural frequencies as a function of the rotor running speed, drawn from our computations are similar to those given in reference [1]. Reference [14] gives a detailed illustration of these examples.

The comparison between vibration responses to imbalance, to asynchronous excitation and to harmonic excitation are also satisfactory. Figures 5 and 6 show an example of the response to harmonic excitation between 0 and 80 Hz of system I (see Figure 7).

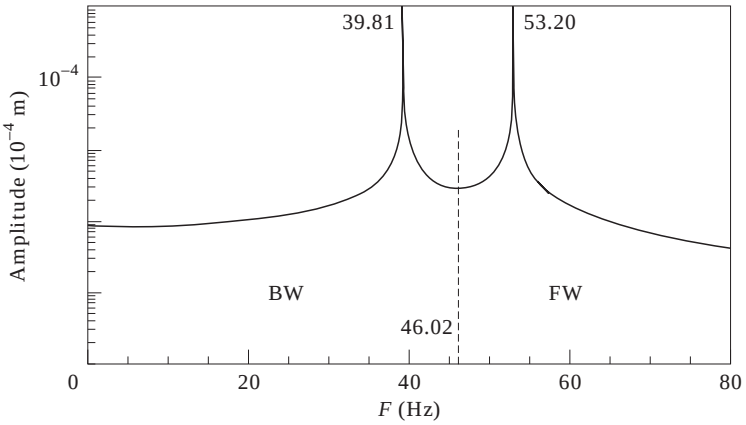

Figure 5. Vibration response to an harmonic excitation (0–80 Hz) of system shown in Figure 7 (reference [1]). Running speed = 2400 r.p.m.

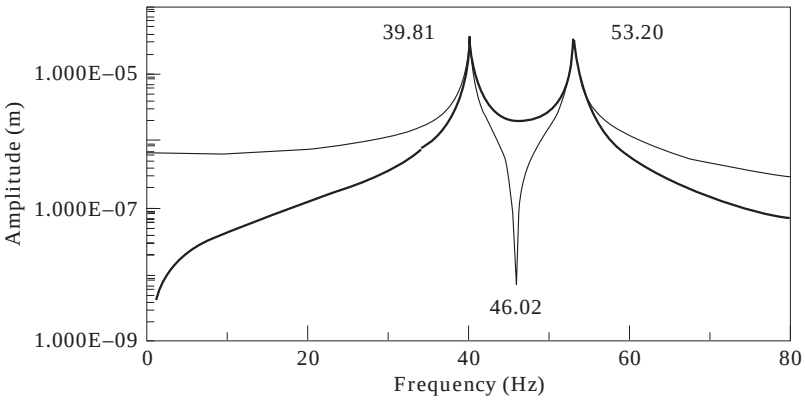

Figure 6. Vibration response to an harmonic excitation (0–80 Hz) of system shown in Figure 7 (our calculation). Running speed = 2400 r.p.m. ——, Along X; ——, along Z.

At steady state, the orbit described by the rotor axis is in most cases an ellipse, one notices (Figure 6) that the rotation can be determined from the antiresonance analysis of the magnitudes along X and Z.

From sensitivity tests performed on vibration parameters one observed the following: natural frequencies are very sensitive to bearing stiffness variations and to the disks and their positions; disks induce important gyroscopic effects, and the disks' positions on the rotor axis are factors of the natural frequency at which this effect appears; the number of critical speeds is higher in the case of non-symmetric rotors (different bearing stiffnesses).

As far as misalignment is concerned (see the Appendix), Figure 8 shows the variation of acceleration magnitudes at running speed and at $n \times$ running speed, calculated at a journal bearing as a function of the misalignment angle α. This computation was done for a system whose first resonance frequency is 110 Hz when $\Omega = 2400$ r.p.m. This result confirms the fact that misalignment produces vibrations such that the amplitude of the $2 \times$ running speed component is predominant. For the components of higher order (4, 5 and $6 \times$ running speed) the effect of misalignment should not be neglected; it could indeed create damage

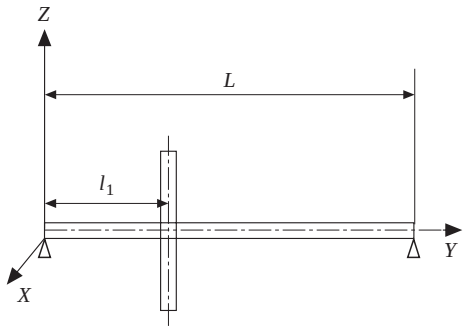

Figure 7. System I. Shaft: $L = 0{\cdot}4$ m, $\phi = 0{\cdot}02$ m, $\rho = 7800$ kg/m^3, $E = 2 \times 10^{11}$ N/m^2. Disk: $\phi_{int} = 0{\cdot}02$ m, $\phi_{ext} = 0{\cdot}3$ m, $h = 0{\cdot}03$ m, $\rho = 7800$ kg/m^3, $l_1 = L/3$. Bearings: $K_X^0 = 10^{11}$ N/m, $K_X^L = 10^{11}$ N/m, $K_Z^0 = 10^{11}$ N/m, $K_Z^L = 10^{11}$ N/m, $C_X^0 = 0$, $C_X^L = 0$, $C_Z^0 = 0$, $C_Z^L = 0$.

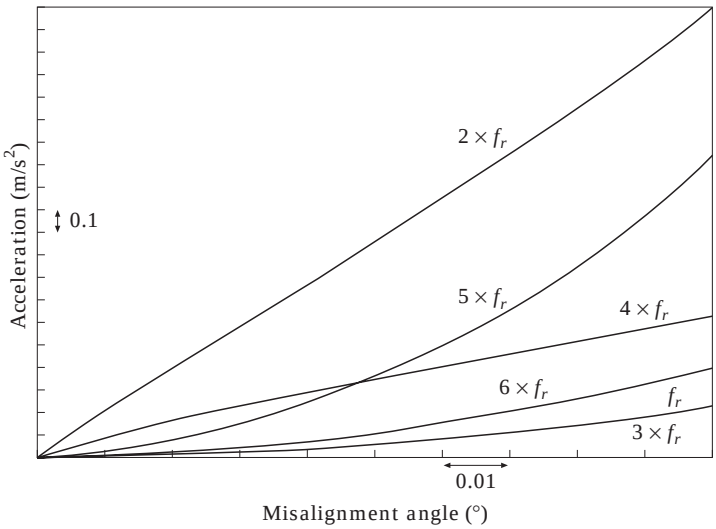

Figure 8. Calculation of the accelerations at $n \times$ running speed (f_r) as a function of the misalignment.

especially if those frequencies coincide with some of the system natural frequencies.

Figure 9 shows a sketch of the system for which a numerical simulation of a configuration of defects was carried out: $m1$, $m2$, and $m3$ represent the applied imbalance. $m1$ and $m2$ are identically placed with respect to the axis while $m3$ is at 180° from $m1$ and $m2$.

Misalignment or the bearing defect is simulated by applying periodically an impulsion on journal A such that the period of application is constant. In this case, the journal stiffness can be monitored in only one direction, X, in order to analyze vibration consequences that can be summarized as follows: the period of excitation of the impact force is predominant for determining the rotor natural frequencies (see Figures 10 and 11); journal stiffness variation is the most influencing factor of the rotor dynamic response (see Figures 12 and 13); imbalance can be easily located by analyzing the journal vibration responses (see Figure 13).

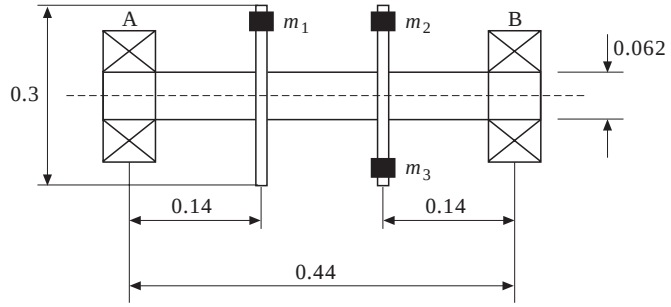

Figure 9. Rotor configuration (shaft + two discs carrying the masses responsible for imbalance) when it rotates in two bearings A and B with the following characteristics: $K_X^A = K_Z^A = K_X^B = K_Z^B = 2 \times 10^{11}$ N/m; $C_X^A = C_Z^A = C_X^B = C_Z^B = 0{\cdot}0$.

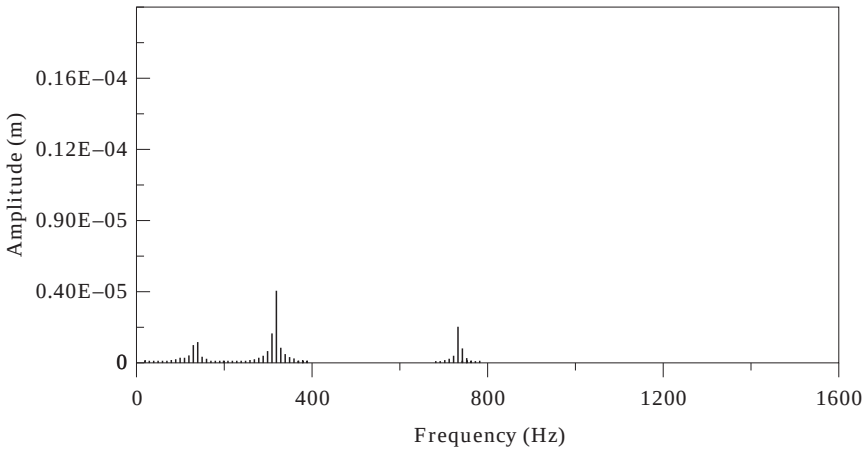

Figure 10. Vibration response at $Y = 0{\cdot}0$ as a function of the frequency. Periodic peak force with $\Delta f = 10$ Hz, magnitude = 4N at $Y = 0{\cdot}0$; running speed = 2400 r.p.m.

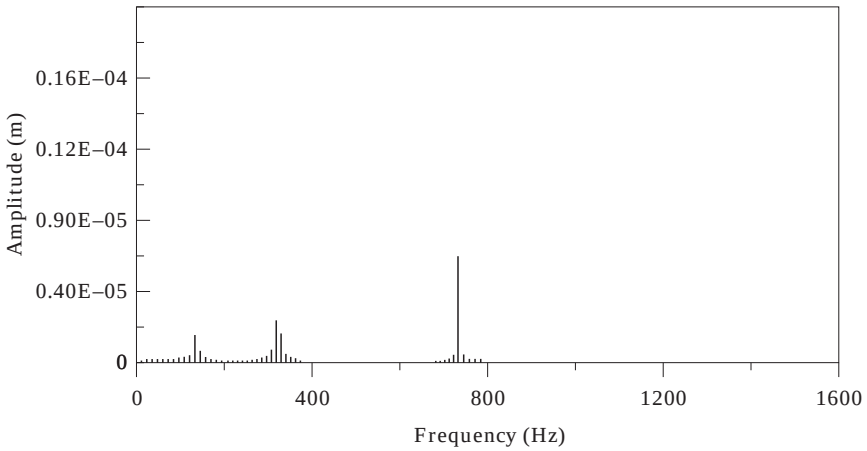

Figure 11. Vibration response at $Y = 0{\cdot}0$, as a function of the frequency. Periodic peak force with $\Delta f = 12$ Hz, magnitude = 4N at $Y = 0{\cdot}0$; running speed = 2400 r.p.m.

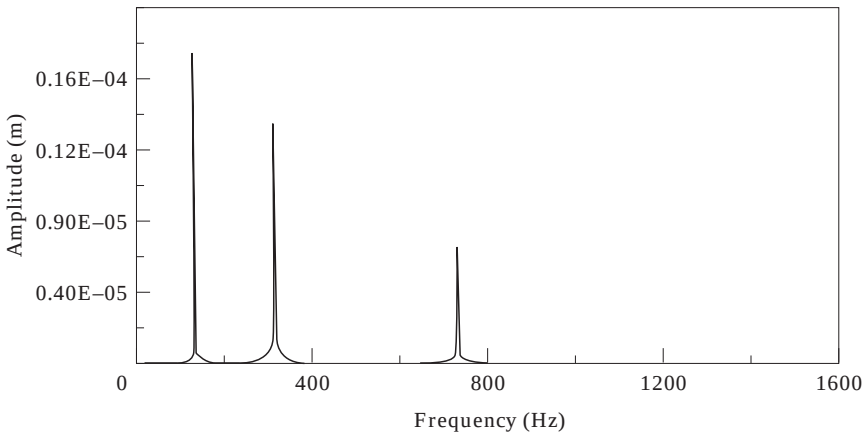

Figure 12. Vibration response at $Y = 0{\cdot}0$, as a function of the frequency. Periodic peak force with $\Delta f = 2$ Hz, magnitude = 4N at $Y = 0{\cdot}0$; running speed = 2400 r.p.m.

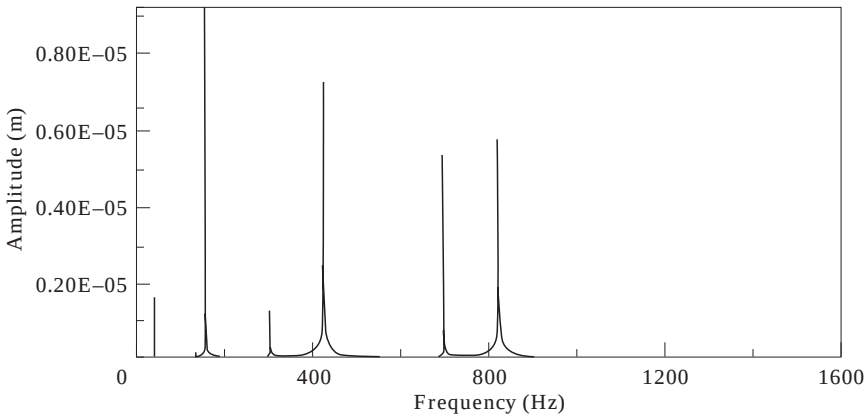

Figure 13. Vibration response at $Y = 0{\cdot}0$ as a function of the frequency. Imbalance $m_1 = 10$ g, Periodic peak force with $\Delta f = 2$ Hz, magnitude = 4N at $Y = 0{\cdot}0$; running speed = 2400 r.p.m. Change in the stiffness of bearing A: $K_X^A = 10^8$ N/m.

4.2. ACOUSTIC CALCULATION

Because it mainly depends on experimental measurements, the pressure calculation with expression (23) is not very accurate. The error ΔP is function of (1) the type of acoustic field around the machine, (2) the mesh used for the computations (N_e), (3) phase variations ($\varphi_{ref} - \varphi_i$), (4) measurement inaccuracies and (5) dipolar effect cancellation at higher frequencies.

Besides the dipolar effect is negligible for frequencies lower than C/L, the effect of other parameters on the calculation of acoustic pressure through sensitivity tests was also analyzed.

Phase variation that yields the complex vibration speeds is the most influential parameter in the calculation of acoustic pressure; the nature of the acoustic field is also important.

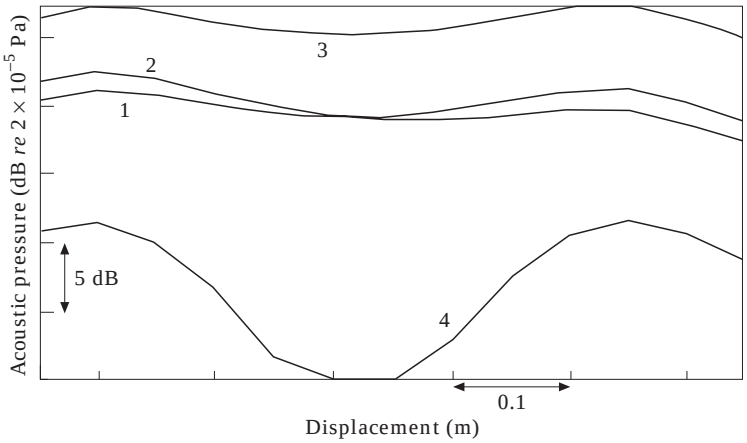

Figure 14. Spatial variations of acoustic pressure level computed for different imbalance types and rotating frequency of 40 Hz. 1. $m_1 = 10$ g, $m_2 = 10$ g; 2. $m_1 = 20$ g, $m_2 = 10$ g; 3. $m_1 = 20$ g, $m_2 = 20$ g; 4. $m_1 = 20$ g, $m_3 = 20$ g.

As far as the mesh of vibrating speeds is concerned, it is related to the rotor bending wavelength. As a consequence, from the second natural frequency, the measurement only of vibrating speed at the journals is not sufficient to describe spatial variations of acoustic pressure.

Calculated acoustic pressure variations were simulated all along the rotor at the running speed for different imbalance configurations (see Figure 14). This calculation is done with a vibration speed acquisition at many points of the rotor–journals system and by affecting a radiating weight to each node of the mesh. The spacial deflection of the calculated pressure is characteristic for each imbalance configuration.

Part II gives an additional analysis comparing theory and experiments.

5. CONCLUSIONS

From a linear dynamic model and a simplified approach to an acoustic study it is possible to define the main mechanical defects in rotating machinery. This straight forward procedure enables one to identify different criteria in order to improve diagnoses and in the end to propose experimental or theoretical procedures to detect the different defects. Before making a comparison with experiments, an analysis of the main parameters led to the following conclusions.

Parameters such as journal stiffness that affects the rotating system transfer function need to be very well known in order to assess the internal force characteristics of the defects.

The acoustic response around the machine is qualitatively well defined but quantitative prediction of noise for vibration analyses is less accurate, the error being due to phase variations between the measured vibration speeds, the type of acoustic field around the machine and the dipolar term being difficult to handle because of the complex geometry.

ACKNOWLEDGMENTS

This work is part of a project with the INRS Nancy and the Campagna & Varenne company. We also acknowledge the support of the Research and Technology Ministry and Work Ministry.

REFERENCES

1. M. Lalanne and G. Ferraris 1990 *Rotor dynamics prediction in engineering*. New York: John Wiley.
2. J. Morel 1992 *Vibrations des machines et diagnostic de leur état mécanique*. Paris: Editions Eyrolles 77.
3. R. Bigret 1980 *Vibrations des machines tournantes et des structures*, *Tome* 1–4. Technique et documentation.
4. M. Xu and R. D. Marangoni 1994 *Journal of Sound and Vibration* **176**, 663–679. Vibration analysis of a motor–flexible coupling–rotor system subject to a misalignment and unbalance, part I: theoretical model and analysis.
5. M. Xu and R. D. Marangoni 1994 *Journal of Sound and Vibration* **176**, 681–691. Vibration analysis of a motor–flexible coupling–rotor system subject to misalignment and unbalance, part II: experimental validation.

6. H. YU and M. L. ADAMS 1989 *Journal of Sound and Vibration* **131**, 367–378. The linear model for the rotor-dynamic properties of journal bearings and seals with combined radial and misalignment motions.
7. D. L. DEWELL and L. D. MITCHELL 1984 *Journal of Vibration, Acoustics, Stress, and Reliability in Design* **106**, 9–16. Detection of a misaligned disk coupling using spectrum analysis.
8. J. DING and J. M. KRODKIEWSKI 1993 *Journal of Sound and Vibration* **164**, 267–280. Inclusion of static indetermination in the mathematical model for non-linear dynamic analysis of multi-bearing rotor systems.
9. J. M. KRODKIEWSKI and J. DING 1993 *Journal of Sound and Vibration* **164**, 281–293. Theory and experiment on a method for on site identification of configurations of multi-bearing rotor systems.
10. N. D. PERREIRA and S. DUBOWSKY 1980 *Journal of the Acoustical Society of America* **67**, 551–563. Analytical method to predict noise radiation from vibrating machine systems.
11. N. HAMZAOUI, C. BOISSON and C. LESUEUR 1992 *Progrès récents des méthodes de surveillance acoustiques et vibrations, conférence internationnale, Senlis, 27–29 octobre*. Modélisation vibroacoustique des défauts sur un rotor.
12. C. FISCHER and V. TERRAIL 1993 *Rapport projet de fin d'etudes, GMC INSA Lyon, juin*. Etude vibroacoustique du mésalignement entre deux paliers.
13. R. D. BLEVINS 1984 *Formulas for natural frequency and mode shape*. Paris: Editions R. E. Krieger.
14. N. HAMZAOUI, C. BOISSON and C. LESUEUR 1990 *Rapport contrat INRS—Campagna et Varenne et INSA*. Dynamique des rotors: modélisation des défauts sur un rotor.
15. C. LESUEUR 1988 *Rayonnement acoustique des structures vibroacoustiques, interactions fluide structure*. Paris: Editions Eyrolles 66.

APPENDIX

If one takes into account some experimental results, a simplified theoretical model can be proposed that yields the vibrations due to a misalignment defect of the receptor shaft bearings (see Figure A1).

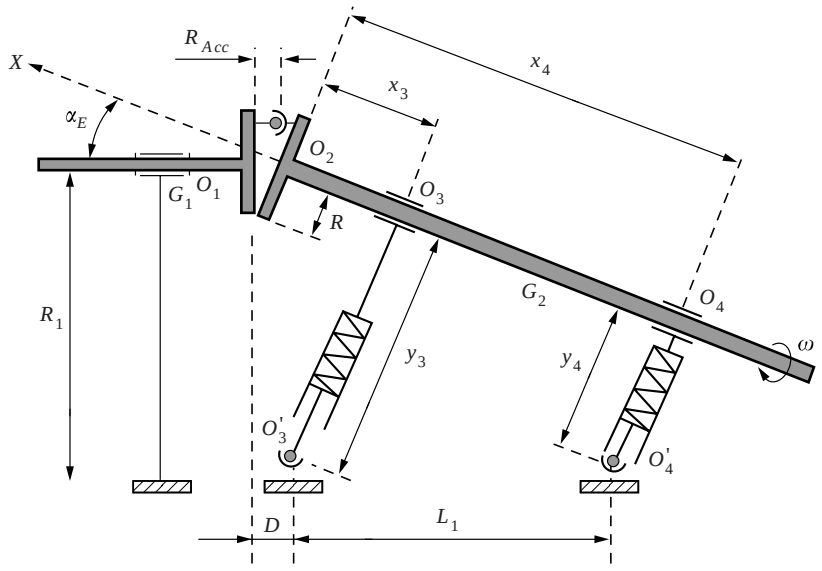

Figure A1. Simplified theoretical model.

The model hypotheses are the following: rigid shafts with constant inertia; the coupling consists of a ball-and-socket joint out of line of the axes intersection; ball bearings are modelled by springs allowing only one translation; the motor shaft is allowed only one rotation around its axis.

Misalignment is imposed as a displacement, and one observes the receptor shaft's position variation around its prescribed position. By writing the system's governing equations, the kinetic energy and deflection equations and by applying Lagrange's equation, one obtains the motion equation $\alpha(t)$ that represents small oscillations around α_E fixed:

$$D(t)\ddot{\alpha}(t) = A(t)\dot{\alpha}(t) + B(t)\alpha(t) + C(t) \tag{A1}$$

Here

$$A(t) = 2m_2R^2\omega \cos \omega t \sin \omega t - \lambda, \tag{A2}$$

m_2 is the shaft mass and λ is the damping factor,

$$D(t) = I_2 + m_2R^2 \cos^2 \omega t + m_2(R_{ACC} + L/2)^2, \tag{A3}$$

$I_2 = \iiint(x^2 + z^2)\,\mathrm{d}m$ is the moment of inertia,

$$\begin{aligned} B(t) = & -m_2R\omega^2(R_{Acc} + L/2)\cos \omega t \sin \alpha_E + m_2R^2\omega^2 \cos \alpha_E \cos^2 \omega t \\ & - K_3[-(D - R_{Acc})(R \cos \omega t + R_1)(2 \sin 2\alpha_E - \sin \alpha_E) \\ & + (D - R_{Acc})^2 \cos 2\alpha_E + (R \cos \omega t + R_1)^2(\cos \alpha_E - \cos 2\alpha_E)] \\ & - K_4[-(D - R_{Acc} + L_1)(R \cos \omega t + R_1)(2 \sin 2\alpha_E - \sin \alpha_E) \\ & + (D - R_{Acc} + L_1)^2 \cos 2\alpha_E \\ & + (R \cos \omega t + R_1)^2(\cos \alpha_E - \cos 2\alpha_E)], \end{aligned} \tag{A4}$$

$$\begin{aligned} C(t) = & -m_2R\omega^2(R_{Acc} + L/2)(1 - \cos \alpha_E)\cos \omega t + m_2R^2\omega^2 \sin \alpha_E \cos^2 \omega t \\ & - K_3[(D - R_{Acc})(R \cos \omega t + R_1)(\cos 2\alpha_E - \cos \alpha_E) \\ & + (D - R_{Acc})^2 \sin 2\alpha_E/2 + (R \cos \omega t + R_1)^2(\sin \alpha_E - \sin 2\alpha_E/2)] \\ & - K_4[(D - R_{Acc} + L_1)(R \cos \omega t + R_1)(\cos 2\alpha_E - \cos \alpha_E) \\ & + (D - R_{Acc} + L_1)^2 \sin 2\alpha_E/2 + (R \cos \omega t + R_1)^2(\sin \alpha_E - \sin 2\alpha_E/2)]. \end{aligned} \tag{A5}$$

In order to obtain the displacement $y_3(t)$ of journal 3 in the model, one uses the linear equation

$$\begin{aligned} y_3(t) = & -[1 - \cos(\alpha_E + \alpha(t))]R \cos \omega t \\ & + R_1 \cos(\alpha_E + \alpha(t)) + (D - R_{Acc}) \sin(\alpha_E + \alpha(t)). \end{aligned} \tag{A6}$$

To solve differential equation (A1), the Runge–Kutta method is used. After replacing $\alpha(t)$, the solution found with Runge–Kutta in equation (A6), one uses a numerical program that develops Fourier transformations and computes the vibration spectrum $y_3(f)$.

Geometrical and mechanical parameters, present in the model, correspond to those of the authors experimental device.

The model transfer function (one degree of freedom) gives 110 Hz as the resonant frequency, this frequency corresponds to the experimental devices. Validity and sensitivity tests on some parameters were performed with satisfaction.

Angular misalignment is such that the $2\times$ and $4\times$ running speed components are predominant. Their magnitudes vary linearly with the misalignment angle. R, the coupling excentricity strongly affects the second harmonic.

In the end, the authors were able to exploit the simplified model although it is still difficult to solve. The next step could be to improve this model by adding one degree of freedom and different stiffnesses to the journals.